Translational Psychiatry

https://doi.org/10.1038/s41398-025-03795-5

Article in Press

Impairment in stimulus-response learning as a cognitive biomarker in a model of synucleinopathy

Received: 8 November 2024

Revised: 3 December 2025

Accepted: 15 December 2025

Cite this article as: Princz-Lebel, O., Attaran, A., Sandoval Contreras, R. *et al.* Impairment in stimulus-response learning as a cognitive biomarker in a model of synucleinopathy. *Transl Psychiatry* (2025). https://doi.org/10.1038/s41398-025-03795-5

Oren Princz-Lebel, Anoosha Attaran, Rodrigo Sandoval Contreras, Vladislav Novikov, Samina Panjwani, Anthony Chu, Cherisse Tan, Claire A. Lemieux, Miguel Skirzewski, Meira M. F. Machado, Joel C. Watts, Jacob A. McPhail, Ariel Louwrier, Vania F. Prado, Lisa M. Saksida, Marco A. M. Prado & Timothy J. Bussey

Title

Impairment in stimulus-response learning as an early cognitive biomarker in a model of synucleinopathy.

Authors

Oren Princz-Lebel[1,2*], Anoosha Attaran[2*], Rodrigo Sandoval Contreras[2], Vladislav Novikov[1,2], Samina Panjwani[1,2], Anthony Chu[1,2], Cherisse Tan[3], Claire A. Lemieux[3], Miguel Skirzewski[2,4], Meira M.F. Machado[2], Joel C. Watts[5,6], Jacob A. McPhail[7,8], Ariel Louwrier[7], Vania F. Prado[1,2,4], Lisa M. Saksida[1,2,3], Marco A.M. Prado[1,2,4], Timothy J. Bussey[1,2,3,9]

Affiliations

1. The Graduate Program in Neuroscience, Schulich School of Medicine and Dentistry, Western University, London Ontario, Canada
2. Robarts Research Institute, Schulich School of Medicine and Dentistry, Western University, London Ontario, Canada
3. Department of Physiology and Pharmacology, Schulich School of Medicine and Dentistry, Western University, London Ontario, Canada
4. Department of Anatomy and Cell Biology, Schulich School of Medicine and Dentistry, Western University, London Ontario, Canada
5. Tanz Centre for Research in Neurodegenerative Diseases, University of Toronto, Toronto, Canada
6. Department of Biochemistry, University of Toronto, Toronto, Canada
7. StressMarq Biosciences, Victoria, British Columbia, Canada
8. Institute for Neurodegenerative Diseases, Weill Institute for Neurosciences, University of California, San Francisco, CA, USA

9. Corresponding author
   Dr. Timothy Bussey
   Translational Cognitive Neuroscience Laboratory
   Schulich School of Medicine and Dentistry
   Western University, London, ON, N6A 3K7
   Phone: +1 5196613452
   Email: tbussey@uwo.ca

* These authors share co-first authorship.

Keywords

α-synuclein, stimulus-response learning, cognition, synucleinopathy, pre-formed fibril, touchscreen

Abstract

Translating findings from preclinical assessments of cognitive function relevant to synucleinopathies into successful clinical trials poses significant challenges. In this study, we examined the effectiveness of human-relevant touchscreen cognitive assessments in detecting the impact of α-synuclein pathology in a mouse model of synucleinopathy on the emergence of stimulus-response learning impairments as a potential cognitive biomarker. We generated two types of α-synuclein pre-formed fibrils, each displaying distinct biophysical characteristics *in vitro* and biochemical properties when stereotaxically injected *in vivo*. These two types of fibrils were capable of triggering impairments in stimulus-response learning in pre-motor, prodromal disease stages, akin to what is observed in humans with synucleinopathy. This work supports the use of touchscreen cognitive assessments in conjunction with robust preclinical rodent models for identifying targets and testing therapeutic strategies for synucleinopathic diseases.

Introduction

Neurological diseases affecting cognition are leading sources of ill health and disability worldwide, making them key public health priorities. Animal models are critical for understanding and developing treatments for these diseases, but present significant challenges as robust, validated animal models must be combined with appropriate, translational, and reliable behavioural assessments to understand how pathology affects cognition[1–4]. One class of neurological disease for which such modelling is currently underdeveloped are the synucleinopathies, which include Parkinson's Disease (PD), Lewy Body Dementia, and Multiple Systems Atrophy. In these diseases, cognitive deficits are highly prevalent, often appear in early prodromal disease stages[5], and have significant impacts on quality of life, disability, and caregiver burden[6,7].

Synucleinopathies are characterized by misfolding, aggregation and propagation of α-synuclein (aSyn)[8]. In its native form, aSyn is a small soluble protein that is predominantly expressed in the presynaptic nerve terminals of mammalian brain tissue[9], and which carries out key regulatory functions that include lipid metabolism and transfer[10–12] as well as synaptic transmission and plasticity[13–16]. In disease states, however, aSyn is known to misfold and aggregate into toxic proteinaceous and membranous inclusions known as Lewy bodies and Lewy neurites, where a large portion of aSyn is phosphorylated at the serine residue 129 (pS129)[17–19]. Several lines of evidence support a prion-like cell-to-cell transmission of misfolded aSyn[20–25]. According to this model, disease-related conformers of aSyn can act as a template or seed to trigger host aSyn to misfold, become pathological, and spread across the central nervous system[26–28]. Notably, brain atrophy and aSyn deposition occur predominately in cortico-basal ganglia- thalamic circuits[29,30], which are key for maintaining cognitive functions[31] and are sensitive to changes in dopaminergic transmission[32,33].

To study synucleinopathies in preclinical models, a widely used and reliable approach is the injection of aSyn pre-formed fibrils (PFF) in the M83 hemizygous transgenic mouse model, which overexpresses human mutant α-synuclein (A53T) and develops progressive neurological symptoms[24,25,34,35]. In this model, aSyn pathology can be induced by injecting fragmented aSyn PFFs composed of human recombinant misfolded aSyn species into the brain, spinal cord, or gut, which initiates the seeding of pathological species near the site of injection, and which can spread within interconnected tissues[24,25,36]. Recently, it has been shown that this model is also capable of

recapitulating the progressive brain atrophy and aSyn deposition in cortico-basal ganglia-thalamic circuits commonly seen in patients[35], along with the development of early-onset deficits in cognitive flexibility[34,35]. Notably, misfolded proteins can assume different conformations that likely contribute to different patterns of diffusion, aggregation, and pathology[37,38]. Indeed, similar to the well-documented prion strains[39,40], aSyn can form multiple conformational strains that can be propagated and selected *in vivo* using the PFF model[37,41,42], enabling the comprehensive study of aSyn pathology under varying misfolding conditions.

One highly translational cognitive construct that is poorly studied in models of synucleinopathy is the acquisition of stimulus-response (S-R) learning. S-R learning is a cognitive process essential for adaptive decision-making and day-to-day functioning, which is commonly impaired in patients with synucleinopathies[43–47], and could serve as a cognitive biomarker. To study S-R learning preclinically in a way that maintains high translational potential, we developed the touchscreen-based Visuomotor Conditional Learning (VMCL) task[48–50]. Notably, VMCL in rodents has been shown to be dependent on relevant nodes within the cortico-basal ganglia-thalamic circuits[51–54], and is sensitive to changes in dopaminergic transmission [55], making it highly relevant for the study of synucleinopathies. Here, we tested whether a combined approach of the robust aSyn PFF model and rodent touchscreen VMCL task could be used to model S-R learning impairments relevant to synucleinopathies.

Materials & Methods

Expression, purification, and fibrilization of α-synuclein

Human aSyn PFF-1 and PFF-2 are available from a commercial source (StressMarq Biosciences Cat# SPR-322 and SPR-317, respectively), which are expressed, purified, and fibrilized using methods previously described[36,56]. In brief, wild-type human aSyn (native, untagged) in a PET24a vector was expressed in *E.coli* BL-21 grown in Terrific Broth with kanamycin. Cultures were grown shaking at 37ºC to an OD_{600} between 0.6-0.9 before induction with 0.2 mM IPTG for overnight expression at room temperature (Type 1, aSyn PFF-1) or 1 mM IPTG for 4 hour expression at 37ºC (Type 2, aSyn PFF-2) before cells were pelleted at 4000 x g, washed with 1X PBS pH 7.4 and frozen -80 ºC. Pellets were boiled at 90 ºC for 15 minutes in 10 mM Tris pH 7.6, 1 mM EDTA and 750 mM NaCl with protease inhibitor cocktail (Sigma Cat #S8820-2TAB) and insoluble material was removed by centrifuging 20,000 x g at 4ºC. Supernatant was incubated with

PEI on ice for 20 minutes and re-centrifuged to precipitate excess nucleic acid. Protein was dialyzed into 10 mM Tris pH 7.6, 1 mM EDTA and 40 mM NaCl overnight at 4ºC. Monomers were purified using anion exchange with a gradient from 40-500 mM NaCl. Fractions containing aSyn visible on SDS-PAGE were buffer-exchanged into 1X PBS pH 7.4. If necessary, monomers were passed through an endotoxin removal column (Pierce) to ensure an endotoxin level <1 EU/mg protein as determined by a ToxinSensor Chromogenic LAL Endotoxin Assay Kit (GenScript). Purified, low endotoxin monomers were concentrated to 5-8 mg/mL using a 5kDa MWCO concentrator (Amicon), filter sterilized (0.2 µm), aliquoted and frozen -80 ºC. Concentration and purity >95% were confirmed by nanodrop and SDS-PAGE. For fibrilization reactions, monomers were thawed, mixed, and centrifuged 20,000 x g at 4ºC to remove any pre-existing aggregate. Supernatant containing monomers was pooled, re-filter sterilized (0.2 µm), and diluted to 5 mg/mL with 1X PBS pH 7.4 if necessary. aSyn was shaken at 37ºC, 1000 rpm for 7 days using a Thermomixer C with a heated lid. Final wild-type human aSyn PFFs were aliquoted and frozen at -80 ºC.

Characterization of α-synuclein PFFs *in vitro*

Sedimentation Assay

PFFs were centrifuged at 20,000 x g at room temperature for 30 minutes. The supernatant was removed and the pelleted PFFs were washed in the same volume of 1X PBS pH 7.4, followed by a re-centrifugation. The wash was removed and final pellet of PFFs were re-suspended in 1X PBS pH 7.4. Supernatant, wash, and pellet samples were re-suspended in loading buffer containing SDS and β-mercaptoethanol and run at 200 V for 50 minutes on a 12% Tris-Glycine SDS-PAGE gel and stained with Coomassie Brilliant Blue G.

Transmission Electron Microscopy

Samples were prepared for examination in the transmission electron microscope using the 'direct application method'[57]. Negative stain transmission electron microscopy images of aSyn PFF-1 and PFF-2 were acquired at 80 Kv on carbon coated 400 mesh copper grids using phosphotungstic acid and uranyl acetate stain.

Thioflavin-T monomer seeding assay

Monomers (100 μM), PFFs (10 μM), or both were shaken at 600 rpm at 37ºC in a sealed Lumox 96-well multiwell plate (Sarstedt Cat# 94.6000.024) for 48 hours in the presence of 25 μM ThT. Fluorescence was measured at regular intervals on a Molecular Devices Gemini XPS Microplate reader using Softmax Pro Software version 6.5.1 at an excitation wavelength of 450nm and an emission wavelength of 485 nm.

Far UV Circular Dichroism

Samples of both aSyn PFF-1 and PFF-2 were initially sonicated 10 cycles at high frequency using a Bioruptor Pico to ensure solubility yet still maintain fibrillar structure. All samples were diluted with 1X PBS buffer to 1.6 mg/mL from 2.0 mg/mL for far-UV analysis. The auto-sampler temperature was set to 20 °C for sample storage prior to injection into the smart cell for analysis at 20 °C. Samples were analyzed on the Chirascan Q100 with monochromator wavelength set at 260.0 nm, bandwidth of 1.0 nm and a step of 0.5 nm, sampling 2 time points per second. Sample spectra were collected in triplicate, averaged, normalized, smooth and converted into CD units of Δε. The CDNN algorithm was used to fit the far-UV CD data for prediction of secondary structure.

Characterization of α-synuclein PFFs *in vivo*

Animals

M83 hemizygous mice (M83+/− mice; B6; C3H-Tg[SNCA]83Vle/J) were obtained from Jackson Laboratory (004479) and maintained in-house on a C57BL/C3H background. These transgenic mice express one copy of the human aSyn transgene array bearing the familial A53T mutation in the SNCA gene under the control of the mouse prion protein promoter, along with endogenous mouse aSyn[58].

Male and female M83 hemizygous (+/−) and littermate controls (−/−), aged 3–6 months, were pseudorandomly assigned to receive intrastriatal injections of wild-type human aSyn PFF-1, PFF-2, or PBS via stereotaxic surgery, with littermates from the same cage distributed across treatment groups to minimize selection and litter-related bias. The distribution of ages was balanced across groups to ensure comparability. For details, refer to the section on stereotaxic surgery for α-synuclein inoculation in the supplementary information.

Experimental Design

Subjects were housed in 28 x 18 cm plastic shoebox cages at 22-23°C, 50 ±10 % humidity with rise tops, and a 12:12h reverse light-dark cycle (lights turned off at 09:00). Food and water were provided *ad libitum* until 1 week prior to behavioural testing, at which point mice were food restricted to 85-90% of their free-feeding body weight. Daily food rations were provided with pellets commercially available from Bio-Serv in Flemington, New Jersey (0.5g Cat#F0171; 1g Cat#F0173). Experiments were performed during the dark cycle (between 09:00-18:00) 5-7 days/ week. Mice were single housed following stereotaxic surgery to prevent infection of the surrounding incision area.

Automated Touchscreen Cognitive Assessment

Apparatus

Cognitive testing was conducted within automated Bussey-Saksida Mouse Touchscreen Systems Model 80614-20 (Lafayette Instruments, Lafayette, IN). Experiments were carried out inside sound-attenuating cabinets which consist of a standard operant chamber and a touch-sensitive 12.1-inch monitor (screen resolution 600 x 800), as previously described[59]. Throughout testing, the touchscreen was permanently covered by a black Plexiglas 3-holes mask, which limited subjects' interaction with the screen to relevant task locations (three 7x7cm square windows). A liquid reward dispensing magazine was situated at the back of the chamber and linked to a liquid reward dispenser pump (reinforcer used: Strawberry milkshake from Neilson Dairy). A light emitting diode (LED) illuminated the food magazine during reward delivery and a tone generator triggered auditory tones used throughout touchscreen training. Animal activity was recorded via infrared photobeams located at the front and back of the chamber and at the entry to the reward magazine. The schedule design, control of the apparatus via Whisker control system and data collection was controlled by ABET II Video Touch software V21.02.26.

Touchscreen habituation and pre-training

Between 2-8 weeks post-injection (WPI), mice were habituated to the touchscreen apparatus. The stages of acclimation and appetitive conditioning is freely available within the standard operating procedure at touchscreencognition.org. In brief, mice were assigned to a specific touchscreen operant chamber and gradually exposed to the apparatus, the reinforcer, and the tone. Subsequently, they learnt to interact with specific areas of the screen to receive a reward and

initiate new trials by nose poking the reward receptacle, with each pretraining stage repeated until mice passed a pre-set criterion.

Visuomotor Conditional Learning (VMCL) task

The touchscreen VMCL task is freely available at DOI: 10.58064/ceae-s252 and was run as previously described[49,50]. In brief, sessions began with the delivery of a reinforcer (800ms pulse feed time, 20µL) in the reward receptacle. Upon exiting of the reward tray, one of two discriminatory stimuli (white icicle (image A) or grey equal sign (image B)) was presented in the centre window. Through trial and error, subjects learnt that presentation image A required an immediate nose poke to the right flanking window for a correct response and delivery of reward, while the presentation of image B required a nose poke to the left flanking window. Both discriminatory stimuli were presented equally throughout the session (15 trials of each, for a total of 30 new trials maximum), and were presented pseudo-randomly so that no image was presented more than 3 times in a row. The time to respond to the discriminatory stimuli was uncapped, but the time to respond to the left or right flanking window was limited to 5-seconds to engender fast and automatic S-R learning behaviour.

A correct response was associated with a light in the reward receptacle, the delivery of 20uL of reinforcer, and a 1000ms tone, followed by a 20-second intertrial interval (ITI). An incorrect response, or a failure to respond within 5-second limited hold (termed a 'missed' trial) led to a time-out period, indicated by a 5-second illumination of the house light, followed by an ITI. To counteract the development of side biases and ensure that subjects received a consistent number of rewards per session, any trial immediately succeeding a time out period was designated a 'correction trial' in which the same image was re-presented. Correction trials were consecutively presented until a correct choice was made. The VMCL task involved a maximum of 30 new (non-correction) trials in each maximum 60-minute session for 20 sessions (5-7 sessions per week, maximum of 1 session per day).

The primary outcomes of VMCL were (a) **accuracy** (percentage of correct responses): $\frac{\#\ correct\ trials}{(\#\ total\ trials - \#\ missed\ trials)}$, (b) **Percentage of missed trials:** $\frac{\#\ missed\ trials}{\#\ total\ trials}$**,** (c) **number of correction trials**, (d) **perseveration index**: $\frac{\#\ correction\ trials}{\#\ incorrect\ trials}$, which uses the number of correction trials as an indication of perseverative behaviour, corrected for the number of correction trials that

would be expected based on performance (as poorly performing animals require more correction trials). Importantly, incorrect trials are defined as errors made on the first choice of a new trial; errors occurring during correction trials are not counted as incorrect trials. (e) **correct touch latency**: time from nose-poking the discriminatory stimulus in the central window to nose poking the correct flanking window), (f) **incorrect touch latency**: time from nose-poking the discriminatory stimulus in the central window to nose poking the incorrect flanking window, and (g) **reward collection latency**: time to nose poke into the reward magazine after giving a correct response on the touchscreen. All data are presented as the mean + SEM, and plotted in 5 blocks of 4 sessions.

Motor Function Battery

Various motor assessments, including forelimb grip force, accelerating rota-rod, and CatWalk XT gait analysis, were conducted at 8 WPI (prior to cognitive testing) and at 16 WPI (following cognitive testing) to evaluate the order of symptom development. The experimenter was blind to the experimental condition during motor assessments, but not during data analysis. More details about the assessment of different motor functions can be found in the supplementary information section.

Tissue Collection and Processing

At 16+ WPI, tissue was collected either for whole brain histology, including immunofluorescence staining, or dissected and stored -80°C for biochemistry including western blotting, proteinase K digestion assay, and dot blot assay. For histology, mice were anesthetized with ketamine (100 $mg.kg^{-1}$)-xylazine (20$mg.kg^{-1}$) and transcardially perfused with ice-cold phosphate-buffered saline (PBS) followed by 4% paraformaldehyde (PFA). Brains were extracted and kept overnight in 4% PFA at 4°C, and then transferred into 30% sucrose solution where they stayed until they were flash-frozen on dry-ice in Tissue-Tek O.C.T. Compound (Sakura, Cat. #4583) for long-term storage at -80°C. Tissue was sliced on a cryostat (Leica CM1950s) in 25µm coronal sections. A subset of sections was reserved for immunofluorescence analyses used in this study. For biochemistry, brains were collected from mice cervically dislocated and rapidly dissected on ice, flash frozen, and store at -80°C. More details about the above procedures are described in the methods section of supplementary information.

Data analysis

Analyses were conducted on GraphPad Prism 9 for macOS Version 9.5.1. Shapiro-Wilk test of normality and the Rout method for identifying outliers (Q=0.1%) were conducted prior to each analysis. If normality failed, data were transformed prior to statistical testing[60]. Differences between two means were examined using paired or unpaired t-tests. When examining 3 or more comparisons, tests of analysis of variance (ANOVA) were employed (one- or two- way with repeated measures), followed by Šídák's multiple comparisons if a significant interaction was revealed. Alternatively, if a dataset had missing values due to the identification of outliers, we compared groups using a repeated measures mixed-effects ANOVA model. If the assumption of homogeneity of variances was violated, Welch's ANOVA was used instead, followed by unpaired t-tests with Welch's correction for post hoc comparisons. Sample sizes were estimated using a partial eta squared (ηp 2) power analysis for repeated measures two-way ANOVA (power = 0.8, $\alpha = 0.05$)[61]. We acknowledge the importance of investigating potential sex differences, and although male and female mice were tested in a balanced design[62], they were combined in statistical analyses due to insufficient power to detect sex differences[63]. Analyses where p values (or adjusted p values) < 0.05 were considered significant.

Results

Generation and characterization of recombinant α-synuclein pre-formed fibrils in vitro.

To examine the effect of aSyn pathology on S-R learning, we first characterized two human recombinant aSyn PFFs *in vitro,* generated by changing the time and temperature for protein expression in *E. coli*. The first fibril type, referred to as PFF-1, was generated from monomers expressed in *E.coli* at room temperature overnight. The second fibril type, referred to as PFF-2, was generated from monomers expressed in *E.coli* at 37ºC for four hours (Fig. 1A). Although fibrils were shaken under the same conditions (1,000 rpm at 37 ºC), they displayed distinct biophysical properties when analysed *in vitro*. Both fibril types were mainly insoluble and appeared as elongated fibrils of mixed lengths under transmission electron microscopy (Fig. 1B-C). Far UV circular dichroism measurements indicated a high β-sheet content in both fibrils compared to disordered monomers, but with some small differences: lower β-sheet/turn content (40.4% vs 43.0%) and random coil content (31.4% vs 33.4%), but higher α-helix content (23.7%

vs 19.6%) was revealed in PFF-1 relative to PFF-2 (Fig. 1D). Differences were observed in Thioflavin-T (ThT) binding between the preparations, with aSyn PFF-1 triggering a stronger ThT signal both after fibrilization and during a seeding assay with additional monomers (Fig. 1E-F). Taken together, despite originating from the same monomeric source expressed in *E.coli* under different conditions, differences in seeding capability and secondary structures support the notion that PFF-1 and PFF-2 may represent distinct conformational states of aSyn PFFs *in vitro*.

Inoculation of α-synuclein pre-formed fibrils in M83 mice in vivo.

To evaluate the impact of these distinct aSyn PFFs *in vivo*, we inoculated 3–6-month-old hemizygous (+/-) M83 male and female mice (Fig. 2A). These mice possess one copy of the A53T-mutant human aSyn transgene array and were chosen as they (a) refrain from exhibiting phenotypes until 20 months of age[42,64], a timepoint far exceeding our experimental timeline, and (b) can propagate human recombinant aSyn[65–67]. Equal amounts (12.5µg) of PFF-1 or PFF-2 were inoculated unilaterally into the right dorsal striatum. As negative controls, M83+/- and M83-/- mice were injected with an equivalent volume of phosphate-buffered saline (PBS) solution. None of the PBS-inoculated mice developed discernable phenotypes at any point during the experiment, and direct comparisons revealed no significant differences in behaviour (Supplementary Fig. 1). For this reason, control groups were combined for behavioural testing. Furthermore, we confirmed that the age distribution was balanced across groups to ensure comparability. We also statistically verified that starting age had no effect on subsequent behavioral performance, as assessed by regression analysis of percent correct accuracy (Supplementary Fig 2).

To evaluate if PFF-1 and PFF-2 would show different biochemical properties upon inoculation *in vivo*, we conducted a comparative analysis of their susceptibility to proteinase K digestion. Sensitivity to proteinase K cleavage typically indicates an unfolded and/or denatured structure of aSyn, whereas resistance suggests a more compact and aggregated conformation[68]. Critically, the pattern of peptide fragments generated by proteinase K digestion can also serve to discriminate conformational strains[37,69]. In support of aSyn PFF-1 and PFF-2 potentially existing as distinct conformational strains *in vivo*, we found that brain homogenates from aSyn-inoculated mice of both fibril types were resistant to proteinase K but exhibited somewhat distinct banding patterns upon digestion (Fig. 2B). While PFF-1 digestion generally produced 1 digestion band, PFF-2 digestion often generated 2 stronger bands. Furthermore, while both fibril types exhibited

significant binding to chBIIB054, an antibody with high affinity for aggregated aSyn[70], aSyn PFF-2-seeded brain homogenates presented with a stronger signal following dotblot analyses (Fig. 2C-D). Taken together, these results suggest that aSyn PFF-1 and PFF-2 may represent distinct aSyn strains upon inoculation *in vivo*.

Propagation of aggregated α-synuclein following inoculation in vivo.

Relative to controls, both aSyn PFF-1- and PFF-2-inoculated mice also exhibited significant pS129 pathology at 16 weeks post-injection (WPI) (Fig. 3). Similar to previous studies[35,71,72], immunohistochemical analyses revealed significant aSyn pS129 inclusions in regions that encompassed, but were not limited to, the injection site (dorsal striatum), the orbitofrontal cortex, piriform cortex, medulla and substantia nigra (Fig. 3C). Qualitatively, inclusions and staining were similar between PFF-1 and PFF-2. To quantify immunoreactivity for pS129 further, detergent-soluble and insoluble aSyn fractions of protein extracts were taken from the striatum (Fig. 3D-I) and cortex (Supplementary Fig. 3) and quantified with immunoblots. pS129 levels from mice inoculated with PFFs were expressed as the percentage change from the levels found in mice inoculated with PBS (controls). However, pS129 levels in cortex and striatum did not differ significantly between PFF-1 and PFF-2 (Fig. 3E-F), as did human aSyn levels (Fig. 3H-I). Together, this work demonstrates that while both types of fibrils induced aSyn pathology, no differences were observed between them with respect to pS129 levels.

Inoculation of α-synuclein PFF-2, but not PFF-1, induce motor deficits within 16 weeks.

To track the progression of symptom development following aSyn inoculation, we then compared motor function prior to (8 WPI) and after cognitive testing (16 WPI). These experiments revealed that aSyn PFF-2-inoculated mice, but not PFF-1-inoculated mice, presented with severe motor deficits in the time frame of the experiment (Fig. 4). For example, the forelimb grip force of aSyn PFF-1 (*N* =25, *n*=11♂, *n*=14♀), PFF-2 (*N* =19, *n*=7♂, *n*=11♀), and PBS-control mice (*N* =30, *n*=17♂, *n*=13♀) was compared. While no differences were revealed between time points for PBS controls and aSyn PFF-1-inoculated mice, aSyn PFF-2 mice exhibited a significant decline in forelimb grip strength at 16 WPI relative to 8 WPI (Fig. 4A-B). Similarly, when examining the latency to fall on an accelerating rota-rod between groups, PFF-2-inoculated mice presented with a significantly shorter latency to fall compared to PFF-1 and PBS control mice at 16 weeks, but not 8 weeks (Fig. 4C-E).

Furthermore, we also tested a subset of subjects on the Catwalk XT for gait analysis (Fig. 4F-I). aSyn PFF-1 (*N* =9, *n*=6♂, *n*=3♀), PFF-2 (*N* =8, *n*=6♂, *n*=2♀), and PBS-control M83 (+/-) mice (*N* = 10, *n*=6♂, *n*=4♀) were assessed as they freely traversed the catwalk runway, and automated gait calculations for stride length (Fig. 4G), swing speed (Fig. 4H) and step cycle (Fig. 4I) were compared. Consistent with the patterns of motor dysfunction described above, aSyn PFF-2 inoculated mice, but not PFF-1 or PBS control mice, displayed abnormal gait at 16 WPI relative to 8 WPI (Fig. 4G-I). These data therefore demonstrate severe motor dysfunction at 16 WPI for aSyn PFF-2-inoculated mice. In stark contrast, however, aSyn PFF-1-inoculated mice displayed motor strength, coordination, and gait equivalent to PBS controls throughout the entirety of experimental timeline. Taken together, this work suggests that aSyn PFF-1 and PFF-2 strains progress at different rates to the final stages of disease.

Inoculation of both α-synuclein PFF-1 and PFF-2 induce stimulus-response learning impairments prior to motor dysfunction.

Finally, we directed our attention towards assessing cognitive function during the interval between motor assessments (9-12 WPI), preceding the presentation of major motor impairments. The VMCL task is a well-established instrumental paradigm which assesses the acquisition and expression of S-R contingencies through the repeated pairing of visual stimuli (presented on a touch-sensitive screen) with arbitrary motor responses (nose pokes to the right- or left-flanking positions). Designed to be solvable by establishing distinct S-R associations, rather than action-outcome strategies or by simple pavlovian conditioning processes alone[54], it has previously been shown to be dependent on the striatum[53,54], cingulate cortex[51], and nigrostriatal dopamine[55], all of which are highly disrupted in patients with synucleinopathies.

At 9-12 WPI, mice inoculated with aSyn PFF-1 (*N* =25, *n*=11♂, *n*=14♀), PFF-2 (*N* =23, *n*=11♂, *n*=12♀), and PBS-control mice (*N* =30, *n*=14♂, *n*=16♀) were tested on the VMCL task (Fig. 5). Relative to PBS controls, both aSyn PFF-1- and PFF-2-inoculated mice were significantly impaired at acquiring the VMCL task, reflected in a 10-20% reduction in their final % correct accuracy in block 5 (Fig. 5B). With chance level performance at 50% (Figure 5C) and the highest controls levels at ~80% (Fig. 5D), this reduction represents about 30-60% of the behavioural range. These mice also performed a greater number of correction trials, achieved a higher perseveration index, and took longer to make incorrect choices, a pattern of behaviour that may suggest a

decreased sensitivity to negative feedback (Fig. 5F-I). PFF-inoculated mice were not globally impaired, however no significant differences between groups were found in the percent missed trials or the latencies to make correct choices and collect reward (Fig. 5E,H, and J), indicating that motivation and general activity were not affected. Taken together, these results suggest that despite behaving as different strains of aSyn, both PFFs induced a robust cognitive deficit, indicating a compromised ability to learn associations between stimuli and responses, with a pattern of behaviour which may suggest abnormal processing of feedback. Furthermore, given the variable level of impact on motor function observed within our experimental timeline, this work also highlights the sensitivity of VMCL task to detect cognitive deficits in prodromal disease stages under variable misfolding conditions.

Discussion

Our primary goal was to test the validity of a cognitive test for detecting impairments in stimulus-response learning, a domain highly relevant to synucleinopathies. Translating findings from tests of cognitive function relevant to synucleinopathies from preclinical to clinical settings has proven difficult, partly due to the dissimilar and poorly replicable cognitive testing methods commonly used in preclinical studies. Moreover, most cognitive tests used in models of neurodegenerative diseases fail to test cognitive domains that are relevant for human disease. Here, we began to address these issues within the context of S-R learning, a highly relevant cognitive function commonly disrupted in patients with synucleinopathies[44–47,73], which relies on vulnerable cortico-basal ganglia- thalamic brain circuits[33,53,74].

Considerable clinical and pathological heterogeneity exists within and among synucleinopathies, which has been linked to the existence of distinct conformational strains of pathological aSyn that cause different disease manifestations[37,41]. To address this, we generated two distinct strains of human recombinant aSyn PFFs by varying preparation conditions. Both fibril types shared key misfolded protein characteristics, including insolubility and high β-sheet content. However, differences in their secondary structures and ThT binding capacity *in vitro*, suggest that the preparation methods yield fibrils with distinct biophysical properties[75].

To evaluate the impact of aSyn PFFs *in vivo*, we subsequently injected them unilaterally into the dorsal striatum of M83 mice hemizygous for the human aSyn A53T mutation[58]. Although these mice do not display any noticeable phenotypes until over 20 months of age[65,67,76], inoculating them

at 3-5 months resulted in hyperphosphorylation of intraneuronal aSyn accumulations resembling inclusions, along with proteinase K resistance and elevated binding with the chBIIB054 antibody[70]. These results align well with those previously observed using the aSyn PFF in the M83 hemizygous mouse model[34,35,77], and support the ability of aSyn PFFs to induce robust aSyn pathology relevant to synucleinopathies. Notably, however, we also observed somewhat distinct banding patterns following proteinase K digestion, suggesting that these aSyn PFFs may have distinct characteristics upon inoculation *in vivo*, potentially leading to varying levels of pathology in rodents.

Our motor and cognitive assessments, which followed previous experimental designs[34,35], provided insights into how distinct aSyn PFF strains may differentially impact neurological function. This approach enabled us to track the progression of symptom onset, considering that cognitive deficits may precede motor dysfunction in patients with synucleinopathies[78]. The observed phenotypic variability, particularly the motor dysfunction seen with aSyn PFF-2 but not PFF-1, highlights the potential for strain-specific pathological effects. It is important to note that the M83 hemizygous model should not be interpreted as a staging model for Parkinson's disease, but rather as a model of synucleinopathy. In line with this, prior work using microPET imaging has shown no significant changes in dopamine transmission in these mice[79], and motor deficits are likely driven by high levels of α-synuclein overexpression in the spinal cord[80]. Therefore, while dopaminergic mechanisms may modulate some behavioural outcomes, spinal cord pathology likely plays a primary role in the motor phenotype observed here. We acknowledge that our interpretation of cognitive impairments is not directly linked to a specific pathological stage. Future work combining behavioural, and pathological measures will be important for defining disease phases more objectively in this model. These findings support the notion that variations in aSyn PFF structure can drive distinct outcomes, potentially mirroring the heterogeneity seen in synucleinopathies. Moreover, the association between higher aSyn levels and motor impairments in PFF-2-inoculated mice underscores the importance of understanding strain-specific differences when modeling disease progression[37-38, 41]. Our findings are consistent with prior studies showing that α-synuclein pathology can disrupt striatal synaptic plasticity and impair both motor and cognitive functions, including visuospatial and associative learning, in rodent models[81–83]. Notably, differences in the site and form of α-synuclein expression have been linked to distinct

patterns of symptom onset and synaptic dysfunction, including early memory deficits following hippocampal α-syn overexpression[84].

Lastly, cognitive testing was assessed using a touchscreen apparatus, a method widely recognized for its efficacy and replicability[3,4]. This method enables the implementation of behavioural paradigms in rodents that closely mimic those used in clinical settings, facilitating high cross-species translation[3,48–50,85]. To study S-R learning preclinically, we developed the VMCL task[48–50], which has recently been shown to rely on brain circuits and neuromodulators vulnerable in synucleinopathies including the striatum[53,74], cingulate cortex[51], and nigrostriatal dopamine[55]. Importantly, S-R learning is highly conserved between rodents and humans[86–89]and is commonly impaired in patients diagnosed with synucleinopathies[44–47,73], although this relationship can be influenced by medication state[90] and the severity of the disease [73,91].

Notably, we observed significant impairments in acquiring the VMCL task in both aSyn PFF-1 and PFF-2 inoculated mice, including impaired reduction in incorrect choice latencies across learning (Fig 5H), and patterns of behaviour that may suggest abnormal processing of negative feedback, without changes in motivation or motor function as measured by correct choice and reward latencies. This latter finding suggests that the observed impairments were due to learning the task itself, although we cannot definitively rule out an explanation in terms of performance of the task (an impairment in decision-making at choice, despite intact but unexpressed learning of the rule). The data clearly indicate that the VMCL task is sufficiently sensitive to detect cognitive impairments in this mouse model, prior to onset of detectable motor dysfunction, in both protein misfolding conditions tested. Furthermore, the idea of altered feedback in these models chimes with recent studies that have demonstrated altered feedback learning in PD patients[92–94], where the processing of positive and negative feedback is influenced by dopaminergic transmission[93]. Further investigation is needed to determine whether abnormal dopaminergic transmission mediates the cognitive deficits observed following aSyn inoculation.

Collectively, while our findings highlight the potential influence of distinct α-synuclein PFF strains on cognitive and motor outcomes, the primary contribution of this study is in validating the translational potential of the VMCL task for assessing cognitive deficits associated with synucleinopathy.

Together, through the comparison of two distinct aSyn PFFs, we highlighted the efficacy of the aSyn PFF in the M83 hemizgous mouse model combined with the use of translational touchscreen cognitive assessments in the study of S-R learning relevant to synucleinopathies. Despite evidence that our two fibril types displayed distinct characteristics *in vitro* and *in vivo*, both induced a severely compromised ability to make associations between stimuli and responses, occurring prior to the onset of motor dysfunction, and thus replicating clinical conditions[5]. Therefore, the combination of robust animal models and appropriate battery of cognitive touchscreen testing can be successfully deployed for the development of much-needed target identification and therapeutic strategy testing to improve the cognitive function of patients diagnosed with devastating synucleinopathies.

Acknowledgements

We thank Jue Fan, Chris Fodor and the Animal Care and Veterinary Services (ACVS) staff at Western University for animal care. OPL received a Natural Science and Engineering Research Council of Canada (NSERC) graduate scholarship along with a Canadian Institutes for Health Research (CIHR) graduate scholarship. AA received Basic Research Fellowship from Parkinson Canada. MS received funding support from the Canada First Research Excellence Fund Accelerator Awards (BrainsCAN). M.A.M.P., V.F.P., L.M.S., T.J.B., and J.C.W. received support from CIHR (PJT 426966, 162431, 159781, 169101, 169048, 169042), NSERC (402524-2013 RGPIN; 03592-2021 RGPIN; 06711-2019 RGPIN; 065772018), Canada First Research Excellence Fund Accelerator Awards (BrainsCAN, Initiative for Translational Neuroscience), TRanslational Initiative to DE-risk NeuroTherapeutics (TRIDENT) New Frontiers in Research Fund (NFRF), Brain Canada, Canada Foundation for Innovation (CFI) fund (43110, 36569, 37479), and Ontario Research Fund. M.A.M.P is a Tier I Canada Research Chair in Neurochemistry of Dementia. L.M.S. is a Tier I Canada Research Chair in Translational Cognitive Neuroscience. T.J.B is a Western Research Chair. J.C.W. is a Tier II Canada Research Chair in Protein Misfolding Disorders.

Conflict of Interest / Declaration of Interests

Jacob A. McPhail generated and characterized the recombinant alpha-synuclein pre-formed fibrils while an employee of StressMarq Biosciences, and Ariel Louwrier is the founder of StressMarq Biosciences. The authors declare that they have no other competing interests.

Timothy J. Bussey and Lisa M. Saksida have established a series of targeted cognitive tests for animals, administered via touchscreen with a custom environment known as the "Bussey-Saksida touchscreen chamber". Cambridge Enterprise, the technology transfer office of the University of Cambridge, supported commercialisation of the Bussey-Saksida chamber, culminating in a license to Campden Instruments. Any financial compensation received from commercialisation of the technology is fully invested in further touchscreen development and/or maintenance.

All other authors declare no competing interests.

Author Contributions Section

Oren Princz-Lebel, Lisa M. Saksida, Marco A.M. Prado, Vania F. Prado and Timothy J. Bussey designed the experiments. Oren Princz-Lebel, Jacob A. McPhail, Ariel Louwrier, Anoosha Attaran, Rodrigo Sandoval Contreras, Vladislav Novikov, Samina Panjwani, Anthony Chu, Cherisse Tan, Claire A. Lemieux, Miguel Skirzewski and Meira M.F. Machado performed experiments. Oren Princz-Lebel, Marco A.M. Prado and Timothy J. Bussey wrote the manuscript, with the support and review of all authors.

Data availability

Data are available in the following repositories: motor behaviours and biochemical and quantifications- https://figshare.com/account/home#/projects/246104. Visuomotor Conditional Learning (VMCL) touchscreen task are available in the MouseBytes repository, at: https://mousebytes.ca/data-link?linkguid=6bfd7a16-52d4-475d-8f2a-e490e601d541 (https://doi.org/10.58064/qh7h-8w97).

Ethics approval and consent to participate

All procedures were conducted in accordance with the relevant guidelines and regulations, including the Canadian Council on Animal Care (CCAC) guidelines, and were approved by the Animal Care and Veterinary Services (ACVS) at Western University (protocol #2020-162 and #2020-163). All methods were performed in compliance with the ARRIVE guidelines.

References

1. Crabbe JC, Wahlsten D, & Dudek BC. Genetics of mouse behavior: interactions with laboratory environment. *Science* **284**, 1670–1672 (1999).

2. Kafkafi N, Agassi J, Chesler EJ, Crabbe JC, Crusio WE, Eilam D, *et al.* Reproducibility and replicability of rodent phenotyping in preclinical studies. *Neurosci Biobehav Rev* **87**, 218–232 (2018).
3. Palmer D, van Rheenen TE, Hodges JR, Cocks K, Balleine BW, Burrows EL, *et al.* Touchscreen cognitive testing: Cross-species translation and co-clinical trials in neurodegenerative and neuropsychiatric disease. *Neurobiol Learn Mem* **182**, 107443 (2021).
4. Sullivan JA, Dumont JR, Memar S, Skirzewski M, Wan J, Mofrad MH, *et al.* New frontiers in translational research: Touchscreens, open science, and the mouse translational research accelerator platform. *Genes Brain Behav* **20**, (2021).
5. Goldman JG, & Postuma R. Premotor and non-motor features of Parkinson's disease. *Curr Opin Neurol* **27**, 434 (2014).
6. Barone P, Erro R, & Picillo M. Quality of Life and Nonmotor Symptoms in Parkinson's Disease. *Int Rev Neurobiol* **133**, 499–516 (2017).
7. Leroi, I., McDonald, K., Pantula, H. & Harbishettar, V. Cognitive impairment in Parkinson disease: impact on quality of life, disability, and caregiver burden. *J Geriatr Psychiatry Neurol* **25**, 208–214 (2012).
8. Kao AW, Racine CA, Quitania LC, Kramer JH, Christine CW, Miller BL. Cognitive and Neuropsychiatric Profile of the Synucleinopathies: Parkinson's Disease, Dementia with Lewy Bodies and Multiple System Atrophy. *Alzheimer Dis Assoc Disord* **23**, 365 (2009).
9. Jakes, R., Spillantini, M. G. & Goedert, M. Identification of two distinct synucleins from human brain. *FEBS Lett* **345**, 27–32 (1994).
10. Galvagnion C, Buell AK, Meisl G, Michaels TCT, Vendruscolo M, Knowles TPJ, *et al.* Lipid vesicles trigger α-synuclein aggregation by stimulating primary nucleation. *Nat Chem Biol* **11**, 229–234 (2015).
11. Galvagnion C, Brown JWP, Ouberai MM, Flagmeier P, Vendruscolo M, Buell AK, *et al.* Chemical properties of lipids strongly affect the kinetics of the membrane-induced aggregation of α-synuclein. *Proc Natl Acad Sci U S A* **113**, 7065–7070 (2016).
12. Sharon R, Bar-Joseph I, Frosch MP, Walsh DM, Hamilton JA, Selkoe DJ. The formation of highly soluble oligomers of α-synuclein is regulated by fatty acids and enhanced in Parkinson's disease. *Neuron* **37**, 583–595 (2003).
13. Cheng F, Vivacqua G, & Yu S. The role of α-synuclein in neurotransmission and synaptic plasticity. *J Chem Neuroanat* **42**, 242–248 (2011).
14. George JM, Jin H, Woods WS, & Clayton DF. Characterization of a novel protein regulated during the critical period for song learning in the zebra finch. *Neuron* **15**, 361–372 (1995).
15. Murphy DD, Rueter SM, Trojanowski JQ, & Lee VMY. Synucleins are developmentally expressed, and alpha-synuclein regulates the size of the presynaptic vesicular pool in primary hippocampal neurons. *J Neurosci* **20**, 3214–3220 (2000).
16. Watson JB, Hatami A, David H, Masliah E, Roberts K, Evans CE, *et al.* Alterations in corticostriatal synaptic plasticity in mice overexpressing human alpha-synuclein. *Neuroscience* **159**, 501–513 (2009).
17. Fujiwara H, Hasegawa M, Dohmae N, Kawashima A, Masliah E, Goldberg MS, *et al.* α-Synuclein is phosphorylated in synucleinopathy lesions. *Nature Cell Biology 2002 4:2* **4**, 160–164 (2002).
18. Uversky VN. A protein-chameleon: conformational plasticity of alpha-synuclein, a disordered protein involved in neurodegenerative disorders. *J Biomol Struct Dyn* **21**, 211–234 (2003).
19. Walker L, Stefanis L, & Attems J. Clinical and neuropathological differences between Parkinson's disease, Parkinson's disease dementia and dementia with Lewy bodies – current issues and future directions. *J Neurochem* **150**, 467–474 (2019).
20. Desplats P, Lee HJ, Bae EJ, Patrick C, Rockenstein E, Crews L, *et al.* Inclusion formation and neuronal cell death through neuron-to-neuron transmission of alpha-synuclein. *Proc Natl Acad Sci U S A* **106**, 13010–13015 (2009).
21. Fares MB, Maco B, Oueslati A, Rockenstein E, Ninkina N, Buchman VL, *et al.* Induction of de novo a-synuclein fibrillization in a neuronal model for Parkinson's disease. *Proc Natl Acad Sci U S A* **113**, E912–E921 (2016).
22. Froula JM, Castellana-Cruz M, Anabtawi NM, Camino JD, Chen SW, Thrasher DR, *et al.* Defining α-synuclein species responsible for Parkinson's disease phenotypes in mice. *Journal of Biological Chemistry* **294**, 10392–10406 (2019).
23. Kordower JH, Chu Y, Hauser RA, Freeman TB, & Olanow CW. Lewy body-like pathology in long-term embryonic nigral transplants in Parkinson's disease. *Nat Med* **14**, 504–506 (2008).

24. Luk KC, Kehm VM, Zhang B, O'Brien P, Trojanowski JQ, Lee VM-Y. *et al.* Intracerebral inoculation of pathological α-synuclein initiates a rapidly progressive neurodegenerative α-synucleinopathy in mice. *J Exp Med* **209**, 975–988 (2012).
25. Luk KC, Kehm V, Carroll J, Zhang B, O'Brien P, Trojanowski JQ, *et al.* Pathological α-synuclein transmission initiates Parkinson-like neurodegeneration in nontransgenic mice. *Science* **338**, 949–953 (2012).
26. Aguzzi A, & Rajendran L. The transcellular spread of cytosolic amyloids, prions, and prionoids. *Neuron* **64**, 783–790 (2009).
27. Jucker M, & Walker LC. Self-propagation of pathogenic protein aggregates in neurodegenerative diseases. *Nature* **501**, 45–51 (2013).
28. Prusiner SB. Cell biology. A unifying role for prions in neurodegenerative diseases. *Science* **336**, 1511–1513 (2012).
29. Angot E, Steiner JA, Hansen C, Li JY, & Brundin P. Are synucleinopathies prion-like disorders? *Lancet Neurol* **9**, 1128–1138 (2010).
30. Braak H, Del Tredici K, Rüb U, de Vos RAI, Jansen Steur ENH, Braak E. Staging of brain pathology related to sporadic Parkinson's disease. *Neurobiol Aging* **24**, 197–211 (2003).
31. Cox J, & Witten IB. Striatal circuits for reward learning and decision-making. *Nature Reviews Neuroscience 2019 20:8* **20**, 482–494 (2019).
32. Reynolds JNJ, & Wickens JR. Dopamine-dependent plasticity of corticostriatal synapses. *Neural Netw* **15**, 507–521 (2002).
33. Wise RA. Dopamine, learning and motivation. *Nature Reviews Neuroscience 2004 5:6* **5**, 483–494 (2004).
34. Lackie RE, de Miranda AS, Lim MP, Novikov V, Madrer N, Karunatilleke NC, *et al.* Stress-inducible phosphoprotein 1 (HOP/STI1/STIP1) regulates the accumulation and toxicity of α-synuclein in vivo. *Acta Neuropathologica 2022 144:5* **144**, 881–910 (2022).
35. Tullo S, Miranda AS, Del Cid-Pellitero E, Lim MP, Gallino D, Attaran A, *et al.* Neuroanatomical and cognitive biomarkers of alpha-synuclein propagation in a mouse model of synucleinopathy prior to onset of motor symptoms. *J Neurochem* **00**, 1–19 (2023).
36. Volpicelli-Daley LA, Luk KC, & Lee VMY. Addition of exogenous α-synuclein preformed fibrils to primary neuronal cultures to seed recruitment of endogenous α-synuclein to Lewy body and Lewy neurite–like aggregates. *Nature Protocols 2014 9:9* **9**, 2135–2146 (2014).
37. So RWL, & Watts JC. α-Synuclein Conformational Strains as Drivers of Phenotypic Heterogeneity in Neurodegenerative Diseases. *J Mol Biol* **435**, (2023).
38. Soto C, & Pritzkow S. Protein misfolding, aggregation, and conformational strains in neurodegenerative diseases. *Nat Neurosci* **21**, 1332 (2018).
39. Safar J, Haeberle H, Deng QC, Leclerc JM, DeArmond JCG, Wille H, *et al.* Eight prion strains have PrPSc molecules with different conformations. *Nature Medicine 1998 4:10* **4**, 1157–1165 (1998).
40. Solforosi L, Milani M, Mancini N, Clementi M, & Burioni R. A closer look at prion strains: Characterization and important implications. *Prion* **7**, 99 (2013).
41. Hoppe SO, Uzunoğlu G, & Nussbaum-Krammer C. α-Synuclein Strains: Does Amyloid Conformation Explain the Heterogeneity of Synucleinopathies? *Biomolecules* **11**, (2021).
42. Lau A, So RWL, Lau HHC, Sang JC, Ruiz-Riquelme A, Fleck SC, *et al.* α-Synuclein strains target distinct brain regions and cell types. *Nature Neuroscience 2019 23:1* **23**, 21–31 (2019).
43. Hadj-Bouziane F, & Boussaoud D. Neuronal activity in the monkey striatum during conditional visuomotor learning. *Exp Brain Res* **153**, 190–196 (2003).
44. Hayes HA, Hunsaker N, & Dibble LE. Implicit Motor Sequence Learning in Individuals with Parkinson Disease: A Meta-Analysis. *J Parkinsons Dis* **5**, 549–560 (2015).
45. Mi TM, Zhang W, McKeown MJ, & Chan P. Impaired Formation and Expression of Goal-Directed and Habitual Control in Parkinson's Disease. *Front Aging Neurosci* **13**, (2021).
46. Olson M, Lockhart TE, & Lieberman A. Motor Learning Deficits in Parkinson's Disease (PD) and Their Effect on Training Response in Gait and Balance: A Narrative Review. *Front Neurol* **10**, (2019).
47. Wu T, Hallett M, & Chan P. Motor automaticity in Parkinson's disease. *Neurobiol Dis* **82**, 226–234 (2015).
48. Bussey T, Muir J, & Robbins T. A novel automated touchscreen procedure for assessing learning in the rat using computer graphic stimuli. *Neurosci Res Commun* (1994).
49. Mar AC, Horner AE, Nilsson SRO, Alsiö J, Kent BA, Kim CH., *et al.* The touchscreen operant platform for assessing executive function in rats and mice. *Nat Protoc* **8**, 1985–2005 (2013).

50. Horner AE, Heath CJ, Hvoslef-Eide M, Kent BA, Kim CH, Nilsson SRO., *et al.* The touchscreen operant platform for testing learning and memory in rats and mice. *Nature Protocols 2013 8:10* **8**, 1961–1984 (2013).
51. Bussey TJ, Muir JL, Everitt BJ. & Robbins TW. Triple dissociation of anterior cingulate, posterior cingulate, and medial frontal cortices on visual discrimination tasks using a touchscreen testing procedure for the rat. *Behavioral neuroscience* **111**, 920–936 (1997).
52. Chudasama Y, Bussey TJ, & Muir JL. Effects of selective thalamic and prelimbic cortex lesions on two types of visual discrimination and reversal learning. *Eur J Neurosci* **14**, 1009–1020 (2001).
53. Delotterie DF, Mathis C, Cassel J-C, Rosenbrock H, Dorner-Ciossek C, Marti A. Touchscreen tasks in mice to demonstrate differences between hippocampal and striatal functions. *Neurobiol Learn Mem* **120**, 16–27 (2015).
54. Reading PJ, Dunnett SB, & Robbins TW. Dissociable roles of the ventral, medial and lateral striatum on the acquisition and performance of a complex visual stimulus-response habit. *Behavioural brain research* **45**, 147–161 (1991).
55. Princz-Lebel O, Skirzewski M, Rai H, Panjwani S, Chu A, Lemieux CA, *et al.* Dissociable patterns of dopamine dynamics and causal contributions to stimulus-response behaviors across striatal subregions. *BioRxiv* (2024) doi:https://doi.org/10.1101/2024.08.16.608313.
56. Polinski NK, Volpicelli-Daley LA, Sortwell CE, Luk KC, Cremades N, Gottler LM, *et al.* Best Practices for Generating and Using Alpha-Synuclein Pre-Formed Fibrils to Model Parkinson's Disease in Rodents. *J Parkinsons Dis* **8**, 303–322 (2018).
57. Doane F, & Anderson N. *Electron Microscopy in Diagnostic Virology : A Practical Guide and Atlas - National Institutes of Health*. (1997).
58. Giasson BI, Duda JE, Quinn SM, Zhang B, Trojanowski JQ, Lee VM-Y. Neuronal α-synucleinopathy with severe movement disorder in mice expressing A53T human α-synuclein. *Neuron* **34**, 521–533 (2002).
59. Kljakic O, Janíčková H, Skirzewski M, Reichelt A, Memar S, El Mestikawy S, *et al.* Functional dissociation of behavioral effects from acetylcholine and glutamate released from cholinergic striatal interneurons. *The FASEB Journal* **36**, (2022).
60. Weiner IB, Freedheim DK, Schinka JA, & Velicer WF. Handbook of psychology. Volume 2, Research methods in psychology. (2003).
61. Lakens D. Calculating and reporting effect sizes to facilitate cumulative science: A practical primer for t-tests and ANOVAs. *Front Psychol* **4**, 62627 (2013).
62. Galea LAM, Choleris E, Albert, A. Y. K., McCarthy, M. M. & Sohrabji, F. The promises and pitfalls of sex difference research. *Front Neuroendocrinol* **56**, (2020).
63. Miller LR, Marks C, Becker JB, Hurn PD, Chen W-J, Woodruff T, *et al.* Considering sex as a biological variable in preclinical research. *The FASEB Journal* **31**, 29 (2017).
64. Watts JC, Giles K, Oehler A, Middleton L, Dexter DT, Gentleman SM, *et al.* Transmission of multiple system atrophy prions to transgenic mice. *Proc Natl Acad Sci U S A* **110**, 19555–19560 (2013).
65. Abdelmotilib H, Maltbie T, Delic V, Liu Z, Hu X, Fraser KB, *et al.* α-Synuclein fibril-induced inclusion spread in rats and mice correlates with dopaminergic Neurodegeneration. *Neurobiol Dis* **105**, 84–98 (2017).
66. Guo JL, Covell DJ, Daniels JP, Iba M, Stieber A, Zhang B, *et al.* Distinct α-synuclein strains differentially promote tau inclusions in neurons. *Cell* **154**, 103 (2013).
67. Luk KC, Covell DJ, Kehm VM, Zhang B, Song IY, Byrne MD, *et al.* Molecular and biological compatibility with host alpha-synuclein influences fibril pathogenicity. *Cell Rep* **16**, 3373 (2016).
68. Aguzzi A, Heikenwalder M, & Polymenidou M. Insights into prion strains and neurotoxicity. *Nature Reviews Molecular Cell Biology 2007 8:7* **8**, 552–561 (2007).
69. Deleersnijder A, Gerard M, Debyser Z, & Baekelandt V. The remarkable conformational plasticity of alpha-synuclein: blessing or curse? *Trends Mol Med* **19**, 368–377 (2013).
70. Weihofen A, Liu YT, Arndt JW, Huy C, Quan C, Smith BA, *et al.* Development of an aggregate-selective, human-derived α-synuclein antibody BIIB054 that ameliorates disease phenotypes in Parkinson's disease models. *Neurobiol Dis* **124**, 276–288 (2019).
71. Arawaka S, Sato H, Sasaki A, Koyama S, & Kato T. Mechanisms underlying extensive Ser129-phosphorylation in α-synuclein aggregates. *Acta Neuropathol Commun* **5**, 48 (2017).
72. Lee HJ, Suk JE, Patrick C, Bae EJ, Cho JH, Rho S, *et al.* Direct Transfer of α-Synuclein from Neuron to Astroglia Causes Inflammatory Responses in Synucleinopathies. *J Biol Chem* **285**, 9262 (2010).

73. Hadj-Bouziane F, Benatru I, Brovelli A, Klinger H, Thobois S, Broussolle E, *et al.* Advanced Parkinson's disease effect on goal-directed and habitual processes involved in visuomotor associative learning. *Front Hum Neurosci* **6**, 33426 (2013).
74. Redgrave P, Rodriguez M, Smith Y, Rodriguez-Oroz MC, Lehericy S, Bergman H, *et al.* Goal-directed and habitual control in the basal ganglia: implications for Parkinson's disease. *Nat Rev Neurosci* **11**, 760 (2010).
75. Burré J, Sharma M, & Südhof TC. Cell Biology and Pathophysiology of α-Synuclein. *Cold Spring Harb Perspect Med* **8**, (2018).
76. Cui G, Jun SB, Jin X, Pham MD, Vogel SS, Lovinger DM, *et al.* Concurrent activation of striatal direct and indirect pathways during action initiation. *Nature 2013 494:7436* **494**, 238–242 (2013).
77. Luk KC, & Lee VMY. Modeling Lewy pathology propagation in Parkinson's disease. *Parkinsonism Relat Disord* **20 Suppl 1**, (2014).
78. Postuma RB, Aarsland D, Barone P, Burn DJ, Hawkes CH, Oertel W, *et al.* Identifying prodromal Parkinson's disease: Pre-Motor disorders in Parkinson's disease. *Movement Disorders* **27**, 617–626 (2012).
79. Levigoureux E, Bouillot C, Baron T, Zimmer L, & Lancelot S. PET imaging of the influence of physiological and pathological α-synuclein on dopaminergic and serotonergic neurotransmission in mouse models. *CNS Neurosci Ther* **25**, (2019).
80. Polinski N. *An Overview of Commonly Used Rodent Models for Studying Alpha-Synuclein*. (2024).
81. Marino G, Campanelli F, Natale G, De Carluccio M, Servillo F, Ferrari E, *et al.* Intensive exercise ameliorates motor and cognitive symptoms in experimental Parkinson's disease restoring striatal synaptic plasticity. *Sci Adv* **9**, (2023).
82. Durante V, de Iure A, Loffredo V, Vaikath N, De Risi M, Paciotti S, *et al.* Alpha-synuclein targets GluN2A NMDA receptor subunit causing striatal synaptic dysfunction and visuospatial memory alteration. *Brain* **142**, (2019).
83. Giordano N, Iemolo A, Mancini M, Cacace F, De Risi M, Latagliata EC, *et al.* Motor learning and metaplasticity in striatal neurons: Relevance for Parkinson's disease. *Brain* **141**, (2018).
84. Iemolo A, De Risi M, Giordano N, Torromino G, Somma C, Cavezza D, *et al.* Synaptic mechanisms underlying onset and progression of memory deficits caused by hippocampal and midbrain synucleinopathy. *NPJ Parkinsons Dis* **9**, (2023).
85. Nithianantharajah J, Komiyama NH, McKechanie AG, Johnstone M, Blackwood DH, Clair DS, *et al.* Bridging the translational divide: identical cognitive touchscreen testing in mice and humans carrying mutations in a disease-relevant homologous gene. *Scientific Reports 2015 5:1* **5**, 1–5 (2015).
86. Dickinson, A. Actions and habits: the development of behavioural autonomy. *Philosophical Transactions of the Royal Society of London. B, Biological Sciences* **308**, 67–78 (1985).
87. Holland PC. Cognitive versus stimulus-response theories of learning. *Learn Behav* **36**, 227–241 (2008).
88. Malvaez M, & Wassum KM. Regulation of habit formation in the dorsal striatum. *Curr Opin Behav Sci* **20**, 67–74 (2018).
89. Ostlund SB, & Balleine BW. Lesions of medial prefrontal cortex disrupt the acquisition but not the expression of goal-directed learning. *J Neurosci* **25**, 7763–7770 (2005).
90. Vo A, Hiebert NM, Seergobin KN, Solcz S, Partridge A, MacDonald PA, *et al.* Dopaminergic medication impairs feedback-based stimulus-response learning but not response selection in Parkinson's disease. *Front Hum Neurosci* **8**, 1–9 (2014).
91. De Wit S, Barker RA, Dickinson AD, & Cools R. Habitual versus goal-directed action control in Parkinson disease. *J Cogn Neurosci* **23**, 1218–1229 (2011).
92. Foerde K, & Shohamy D. The role of the basal ganglia in learning and memory: Insight from Parkinson's disease. *Neurobiol Learn Mem* **96**, 624 (2011).
93. Volpato C, Schiff S, Facchini S, Silvoni S, Cavinato M, Piccione FC, *et al.* Dopaminergic medication modulates learning from feedback and error-related negativity in parkinson's disease: A pilot study. *Front Behav Neurosci* **10**, 213955 (2016).
94. Weismüller B, Ghio M, Logmin K, Hartmann C, Schnitzler A, Pollok B, *et al.* Effects of feedback delay on learning from positive and negative feedback in patients with Parkinson's disease off medication. *Neuropsychologia* **117**, 46–54 (2018).

Figure Legends

Figure 1 | Generation and characterization of recombinant human α-synuclein pre-formed fibrils *in vitro.*

(A) Schematic of α-synuclein pre-formed fibril production. α-synuclein type 1 pre-formed fibrils (PFF-1) were generated from monomers expressed in *E.coli* at room temperature overnight, while α-synuclein type 2 pre-formed fibrils (PFF-2) were generated from monomers expressed in *E.coli* grown at 37^{o}C for four hours. Following this, both fibril precursors underwent monomer purification and identical fibrilization protocols and were characterized *in vitro*. **(B)** SDS-PAGE of PFF-1 and PFF-2 after sedimentation revealed similar populations of insoluble (pellet) vs soluble (supernatant) materials, both consisting of predominantly insoluble species. **(C)** Transmission Electron Microscopy (TEM) of unsonicated PFF-1 and PFF-2 displayed similar architecture and range of fibril sizes, both appearing as elongated fibrils of mixed length. **(D)** Far UV circular dichroism (UV-CD) measurements identified a significant β-sheet presence in fibrils compared monomers with subtle differences between PFF-1 and PFF-2s. Thioflavin T (ThT) binding assay revealed a stronger binding capacity of PFF-1 **(E)** relative to PFF-2 **(F)** after fibrilization and during a seeding assay with additional monomer.

Figure 2 | Experimental design for inoculating α-synuclein pre-formed fibrils in M83 mice *in vivo*.

(A) M83 mice underwent stereotaxic surgery for inoculation of aSyn PFF-1, aSyn PFF-2 or PBS control into the right dorsal striatum. At 8 weeks post injection, they subsequently underwent a motor test battery, including assessments of motor strength, motor coordination and gait. Following completion, they were assessed for the cognitive ability to acquire stimulus-response associations, with the 'Visuomotor Conditional Learning' at 9-12 weeks post injection. At 16 weeks post-injection, they repeated the motor test battery, and then were processed for pathology and biochemistry. **(B)** Brain homogenates from aSyn PFF-1 and PFF-2 inoculated mice both displayed resistance to proteinase K but exhibited variable banding patterns upon digestion, as assessed by Western Blot using an antibody for total aSyn. **(C-D)** Furthermore, the same brain homogenates were evaluated by dotblots using an antibody with high affinity for aggregated aSyn (chBIIB054), revealing that while both fibril types exhibited significant binding, aSyn PFF-2 brain homogenates presented with a stronger signal (Welch's ANOVA test, $W_{2,\ 5.34} = 7.03$, $p<0.05$, in

which Welch-corrected unpaired t-tests revealed to be driven by a significant difference between PBS control and PFF-2 ($p<0.05$). Graphics made with Biorender.com

Figure 3 | Propagation of aggregated α-synuclein following inoculation of pre-formed fibrils in vivo.

(A) aSyn PFF-1, PFF-2 or PBS control was unilaterally injected into the right dorsal striatum. Brains for immunohistochemistry **(B-C)** and immunoblots **(D-M)** were collected at 16 weeks post injection. **(B)** Immunostained brain slices imaged at 63X on a Leica Stellaris 5 Confocal Microscope for aSyn phosphorylated at S129 (green= pS129; blue= Hoescht), scale bar 25µm. **(C)** Although inoculation was localized within the dorsal striatum, pathology spread to many areas including orbitofrontal cortex, piriform cortex, medulla, and substantia nigra. 40X, Leica Stellaris 5 Confocal Microscope, scale bar 50µm. **(D-I)** To quantify this pathology further, protein extract from the striatum of PFF- and PBS-inoculated mice were extracted and quantified with immunoblots**. (D-F)** The levels of pS129 and total human aSyn found in the detergent-soluble (RIPA) fractions from PFF-1 and PFF-2 samples were expressed as the percentage fold change relative to PBS samples. No significant differences were found between PFF-1 and PFF-2 when comparing pS129 (unpaired t-test, $p>0.05$) or human aSyn (unpaired t-test, $p>0.05$). **(G-I)** The levels of pS129 and total human aSyn found in the detergent-insoluble fractions (UREA solubilization of RIPA-insoluble pellets) were expressed in the same way as the detergent-soluble fractions (RIPA). No significant differences were found between PFF-1 and PFF-2 when comparing pS129 (unpaired t-test, $p>0.05$) or human aSyn (unpaired t-test, $p>0.05$). Graphics made with Biorender.com.

Figure 4 | Inoculation of aSyn PFF-2, but not PFF-1, induce motor deficits within 16 weeks.

(A) Schematic of the forelimb grip force test, used to measure muscle strength. Subjects grasped a smooth, triangular pull bar with both forelimbs and the force exerted in Newtons (N) was measured. **(B)** aSyn PFF-2 but not PFF-1 inoculated mice displayed a significant reduction in forelimb muscle strength at 16 weeks post injection (WPI) relative to 8 (2-way RM ANOVA, Group x Session: main effect of group ($F_{2,72}= 4.409$, $p<0.05$), main effect of session ($F_{1,72}= 13.51$, $p<0.001$), and significant interaction ($F_{2,72}= 6.677$, $p<0.01$), in which Šídák's multiple comparisons revealed to be driven by a significant difference within between 8 and 16 weeks within the PFF-2 group (adj. $p<0.0001$). **(C)** Schematic of the accelerating Rota-rod, used to measure motor

coordination and motor learning. Subjects were placed on a stationary rod which began to accelerate linearly from 5-36 revolutions per minute over 5 minutes, and latency to fall (s) was calculated automatically. **(D)** No significant difference between groups was found at 8 WPI (2-way RM ANOVA, Group x Session: main effect of session ($F_{9,675}$= 15.41, p<0.0001), but no main effect of group (p>0.05). A significant interaction was first observed, ($F_{18, 675}$= 1.767, p<0.05), but Šídák's multiple comparisons revealed no significant differences between groups (adj. p>0.05)). However, **(E)** aSyn PFF-2 mice exhibited a shorter latency to fall at 16 WPI relative to aSyn PFF-1 and PBS controls (2-way RM ANOVA, Group x Session: Main effect of group ($F_{2,71}$= 7.436, p<0.01), main effect of session ($F_{9,639}$= 3.205, p<0.001), but no interaction (p>0.05). To examine this main effect further, Šídák's multiple comparisons revealed a significant difference between aSyn PFF-2 and PBS controls (adj. p<0.01) and aSyn PFF-2 and PFF-1 (adj. p<0.01)). **(F)** Schematic of the catwalk XT Gait Analysis, used to measure gait and locomotion. Footprints were captured while subjects voluntarily traversed a glass-plated CatWalk runway, towards a dark goal box at the end. **(G)** A significant difference between 8 and 16 weeks was revealed in the stride length of aSyn PFF-2 inoculated mice (2-way RM ANOVA, Group x Session: no main effect of group (p>0.05), but a main effect of session ($F_{1,24}$= 4.493, p<0.05), and significant interaction ($F_{2,24}$= 3.646, p<0.05), in which Šídák's multiple comparisons revealed a significant difference between timepoints within the aSyn PFF-2 group (adj. p<0.01). **(H)** A significant difference between 8 and 16 weeks was revealed in the swing speed of aSyn PFF-2 inoculated mice (2-way RM ANOVA, Group x Session: no main effect of group (p>0.05), but a main effect of session ($F_{1,24}$= 6.537, p<0.05), and significant interaction ($F_{2,24}$= 4.300, p<0.05) in which Šídák's multiple comparisons revealed a significant difference between timepoints within the aSyn PFF-2 group (adj. p<0.01). **(I)** A significant difference between 8 and 16 weeks was revealed in the step cycle of aSyn PFF-2 inoculated mice (2-way RM ANOVA, Group x Session: no main effect of group (p>0.05), but a main effect of session ($F_{1,24}$= 9.232, p<0.01) and significant interaction ($F_{2,24}$= 4.035, p<0.05) in which Šídák's multiple comparisons revealed a significant difference between timepoints within the aSyn PFF-2 group (adj. p<0.01). Data presented as Mean + SEM, group x session Two-way RM ANOVA, ** p<0.01, **** p<0.0001. Graphics made with Biorender.com

Figure 5 | Inoculation of both α-synuclein pre-formed fibrils induce severe stimulus-response learning cognitive impairments in M83 mice.

(A) Schematic of Visuomotor Conditional Learning (VMCL) task. Cognitive assessments were conducted within touchscreen systems equipped with a touch-sensitive screen, a reward magazine attached to a reward pump for delivery of strawberry milkshake liquid reward and ABET cognition software (*above*). VMCL was employed to evaluate the acquisition of stimulus-response (S-R) contingencies, with subjects learning the conditional rule: "if visual stimulus A is presented, make motor response to the right-flanking window; if visual stimulus B is presented, make motor response to the flight-flanking window" (*below*). All subjects underwent VMCL testing for 20 sessions, 5-7 sessions per week. **(B)** M83 mice inoculated with aSyn PFF-1 and PFF-2 were significantly impaired at acquiring VMCL, as demonstrated by lower percent correct responses relative to PBS-inoculated mice (2-way RM ANOVA, Group x Session: main effect of group ($F_{2,60=10.53}$, $p<0.001$), main effect of session ($F_{2.686,\ 161.2=10.53}$, $p<0.0001$) and significant interaction ($F_{8,240=3.131}$, $p<0.01$), in which Šídák's multiple comparisons revealed to be driven by a significant difference between PBS control and PFF-1 in sessions 2 (adj. $p<0.05$), 4 (adj. $p<0.05$) and 5 (adj. $p<0.05$), and a significant difference between PBS control and PFF-2 in sessions 2 (adj. $p<0.01$), 3 (adj. $p<0.001$), 4 (adj. $p<0.01$), and 5 (adj. $p<0.01$)). **(C)** While all groups began at chance in Block 1 (1-way ANOVA, $p>0.05$), **(D)** both aSyn-inoculated groups were significantly impaired relative to controls in Block 5 (1-way ANOVA, $F_{8.764}$, $p<0.001$, in which Šídák's multiple comparisons revealed to be driven by a significant difference between PBS controls and PFF-1 (adj. $p<0.05$), and between PBS controls PFF-2 (adj. $p<0.001$)). **(E)** No significant difference was found in the percentage of missed trials across groups (RM Mixed-Effects Model, Group x Session: main effect of session ($F_{2.050,118.4=\ 20.55}$, $p<0.0001$), but no main effect of group or interaction ($p>0.05$)), **(F)** but aSyn PFF-1 and PFF-2 mice exhibited a greater number of correction trials (2-way RM ANOVA, Group x Session: main effect of group ($F_{2,60=\ 6.008}$, $p<0.01$), main effect of session ($F_{3.240,194.4=\ 66.22}$, $p<0.0001$) but no interaction ($p>0.05$)), and **(G)** an elevated perseveration index compared to controls (RM Mixed-Effects Model, Group x Session: main effect of group ($F_{2,60=4.648}$, $p<0.05$), main effect of session ($F_{3.191,171.5=24.48}$, $p<0.0001$), but no interaction ($p>0.05$)). Furthermore, comparing task latencies, no significant difference was found in the latency to make correct choices **(H)** (2-way RM ANOVA: Group x Session: $p>0.05$), but aSyn PFF-1 and PFF-2 mice took significantly longer to make incorrect choices **(I)** across VMCL acquisition compared to PBS controls (2-way RM ANOVA: Group x Session: main effect of group ($F_{2,60=5.384}$, $p<0.01$), main effect of session ($F_{3.202,192.1=\ 62.37}$, $p<0.0001$), and significant interaction

($F_{8,240=1.985}$, $p<0.05$), in which Šídák's multiple comparisons revealed to be driven by a significant difference between PBS control and PFF-1 in sessions 2 (adj. $p<0.01$), 3 (adj. $p<0.01$) and 5 (adj. $p<0.05$), and a significant difference between PBS control and PFF-2 in sessions 3 (adj. $p<0.05$) and 5 (adj. $p<0.05$)). No significant difference was found for the latency to collect rewards **(J)** (2-way RM ANOVA, Group x Session: main effect of session ($F_{2.275,135.9=17.67}$, $p<0.0001$), but no main effect of group or interaction ($p>0.05$)). Data presented as Mean + SEM, * $p<0.05$, ** $p<0.01$, *** $p<0.001$. Graphics made with Biorender.com

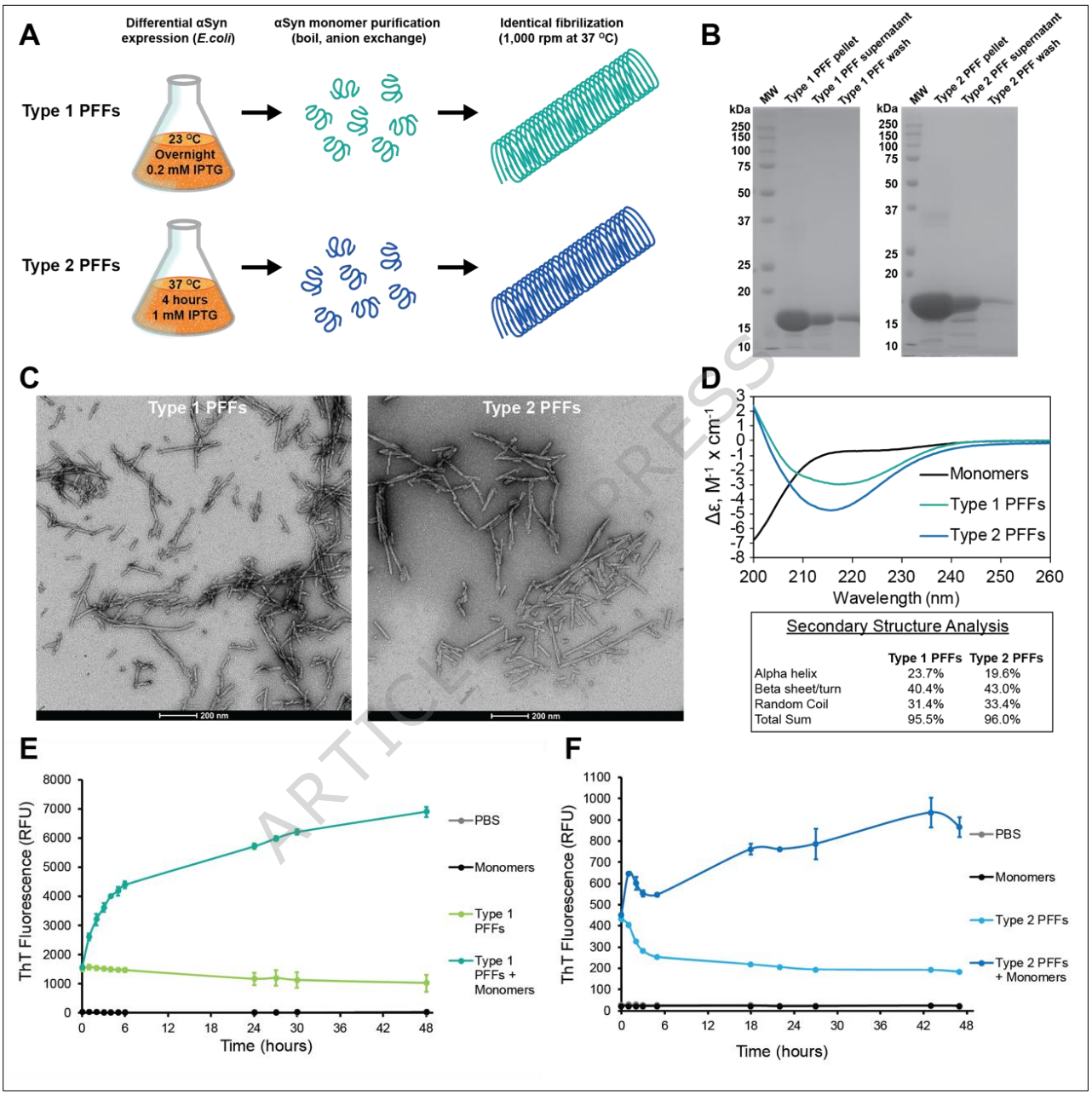
A
Differential αSyn expression (E.coli)
αSyn monomer purification (boil, anion exchange)
Identical fibrilization (1,000 rpm at 37 °C)
Type 1 PFFs
23 °C
Overnight
0.2 mM IPTG
Type 2 PFFs
37 °C
4 hours
1 mM IPTG
B
MW
Type 1 PFF pellet
Type 1 PFF supernatant
Type 1 PFF wash
Type 2 PFF pellet
Type 2 PFF supernatant
Type 2 PFF wash
kDa
250
150
100
75
50
37
25
20
15
10
C
Type 1 PFFs
Type 2 PFFs
200 nm
D
Δε, M⁻¹ x cm⁻¹
Wavelength (nm)
Monomers
Type 1 PFFs
Type 2 PFFs
Secondary Structure Analysis
Type 1 PFFs
Type 2 PFFs
Alpha helix
23.7%
19.6%
Beta sheet/turn
40.4%
43.0%
Random Coil
31.4%
33.4%
Total Sum
95.5%
96.0%
E
ThT Fluorescence (RFU)
Time (hours)
PBS
Monomers
Type 1 PFFs
Type 1 PFFs + Monomers
F
ThT Fluorescence (RFU)
Time (hours)
PBS
Monomers
Type 2 PFFs
Type 2 PFFs + Monomers

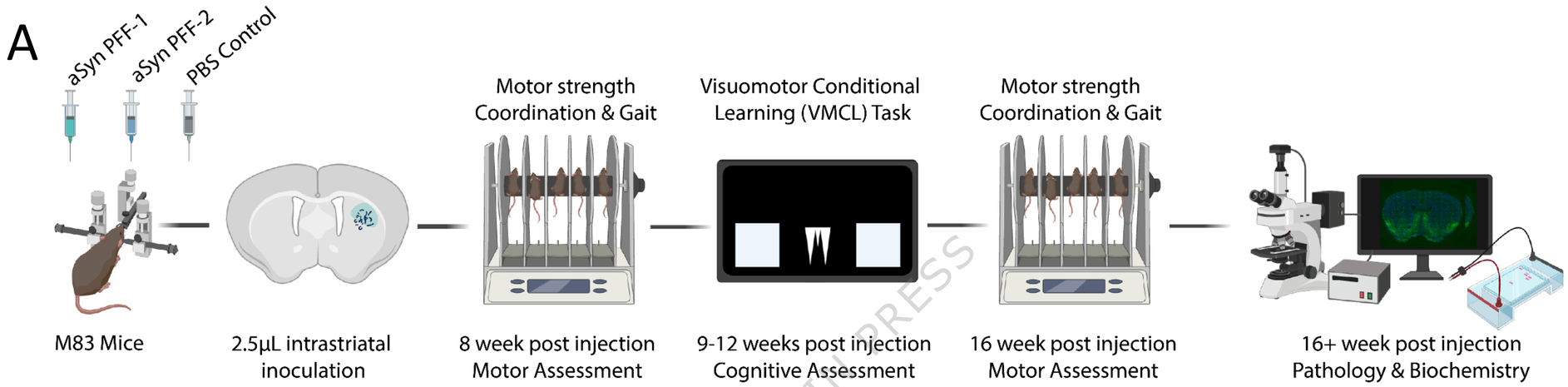
A
aSyn PFF-1
aSyn PFF-2
PBS Control
M83 Mice
2.5µL intrastriatal inoculation
Motor strength Coordination & Gait
8 week post injection Motor Assessment
Visuomotor Conditional Learning (VMCL) Task
9-12 weeks post injection Cognitive Assessment
Motor strength Coordination & Gait
16 week post injection Motor Assessment
16+ week post injection Pathology & Biochemistry

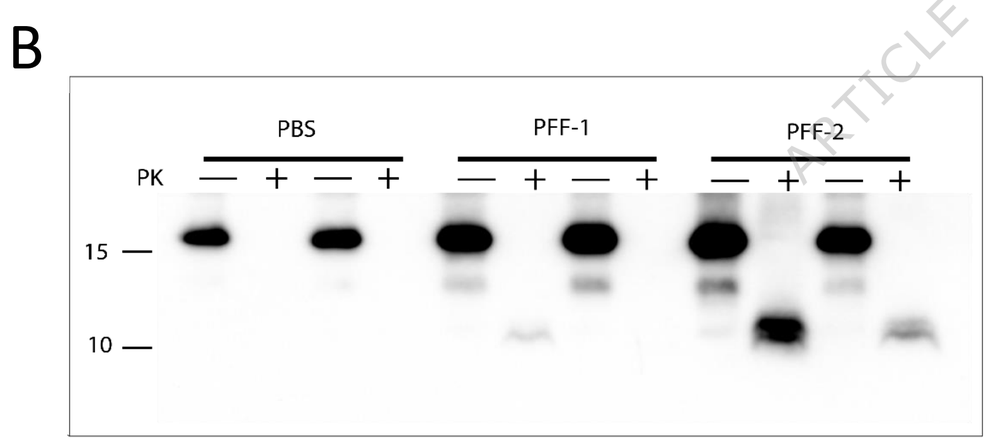
B
PBS
PFF-1
PFF-2
PK
— + — + — + — + — + — + — +
15
10

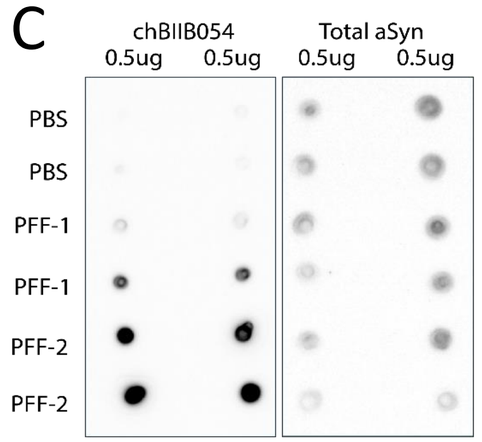
C
chBIIB054
0.5ug 0.5ug
Total aSyn
0.5ug 0.5ug
PBS
PBS
PFF-1
PFF-1
PFF-2
PFF-2

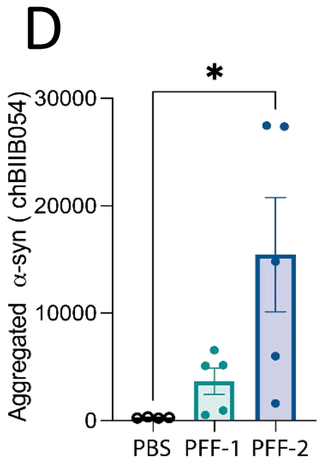
D
*
Aggregated α-syn (chBIIB054)
30000
20000
10000
0
PBS
PFF-1
PFF-2

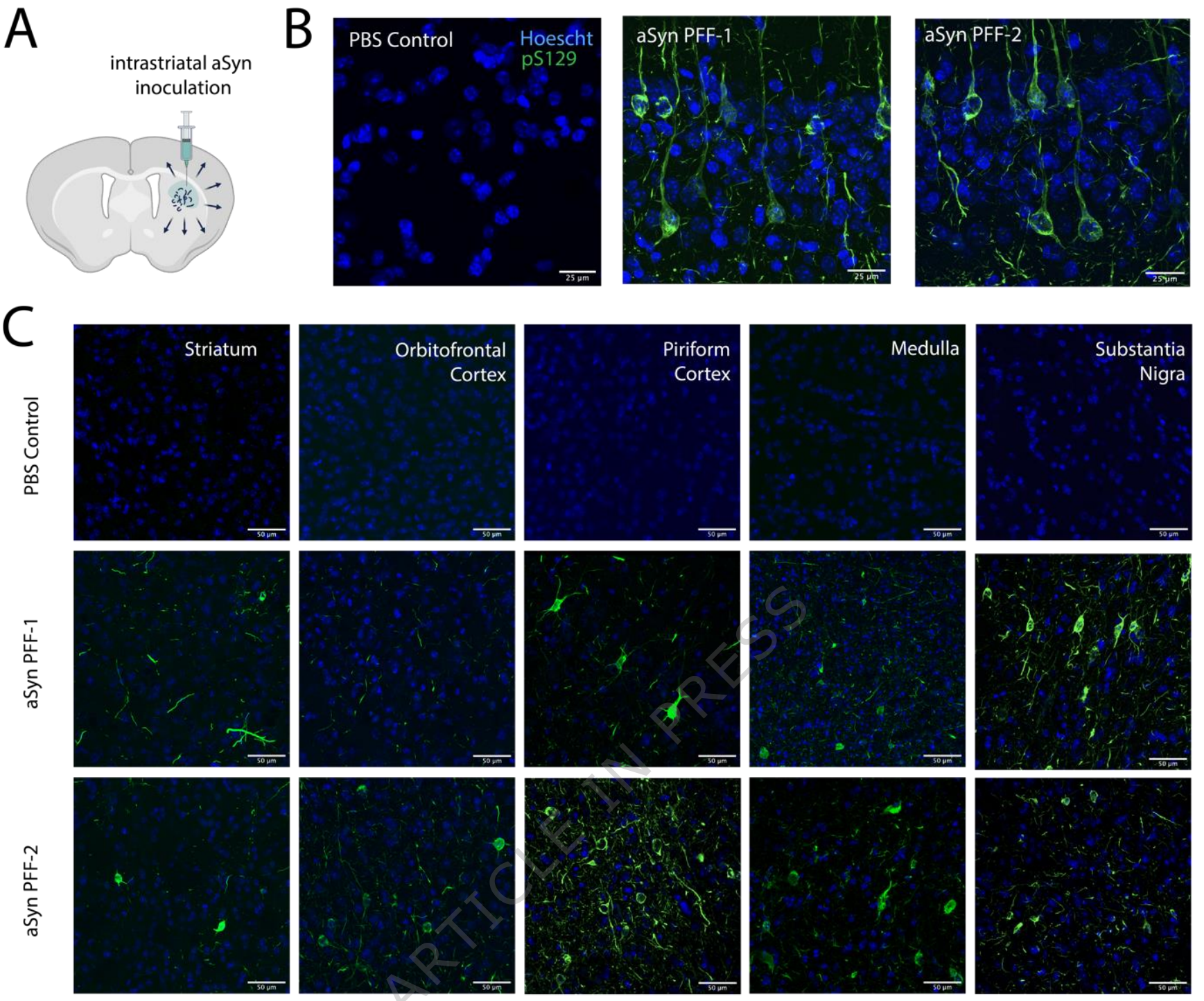

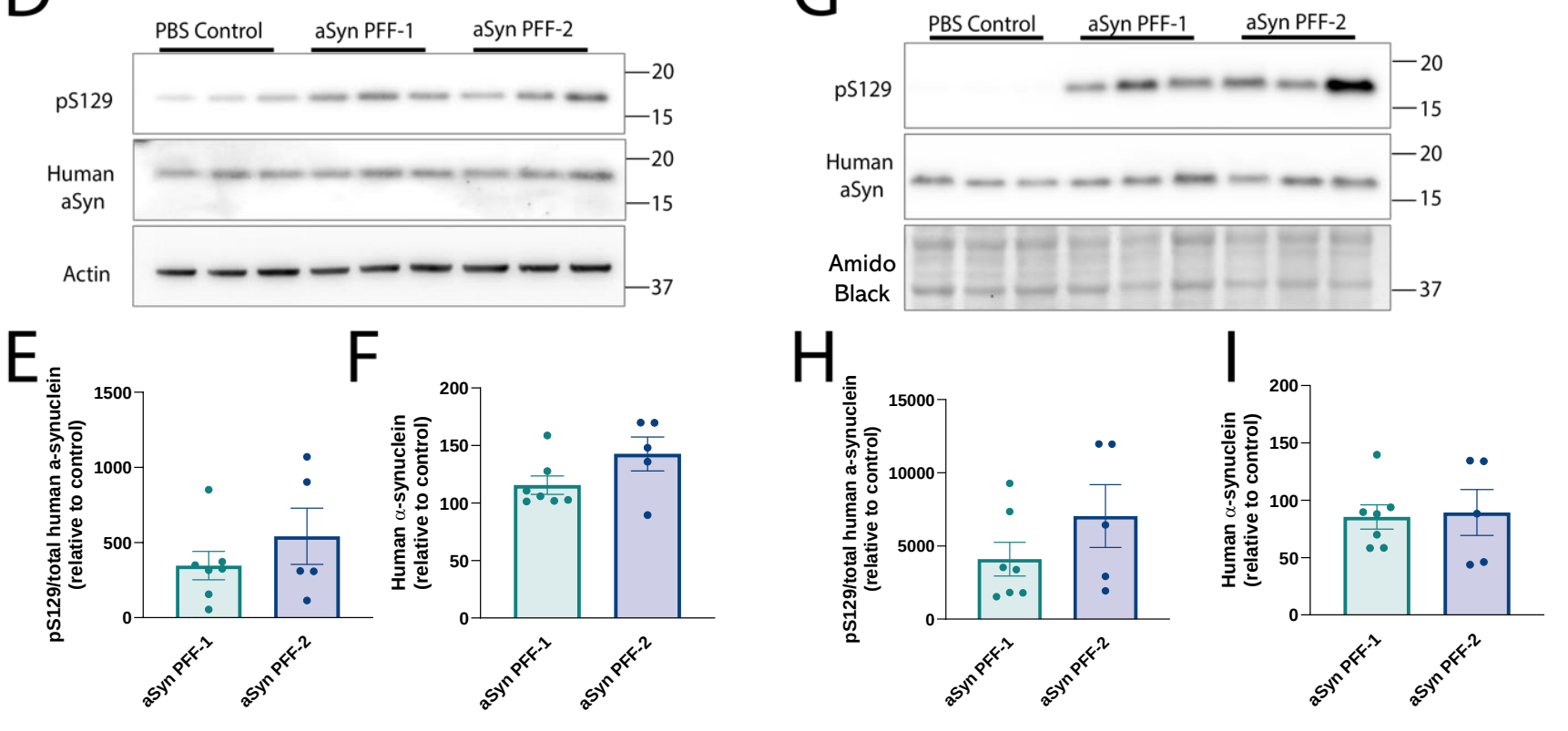

A Forelimb Grip Force

B

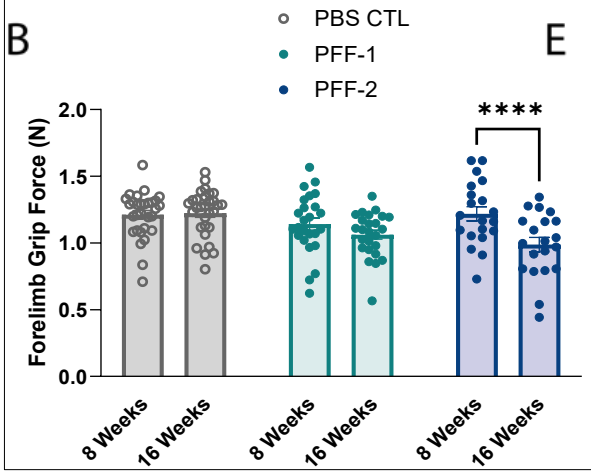

C Accelerating Rota-rod

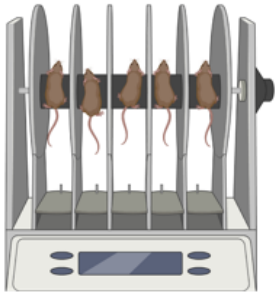

D

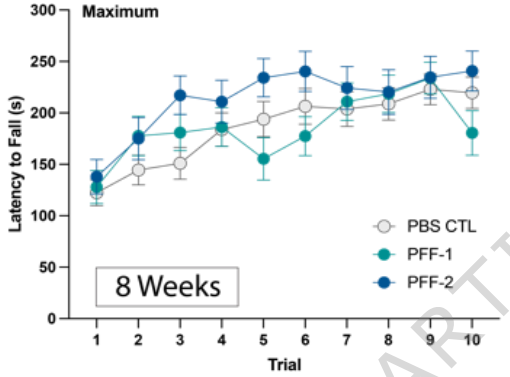

E

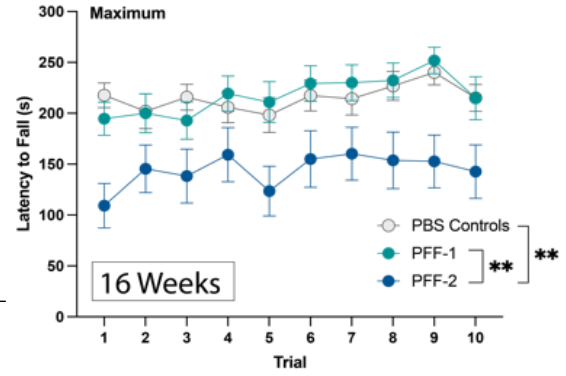

F Catwalk XT Gait Analysis

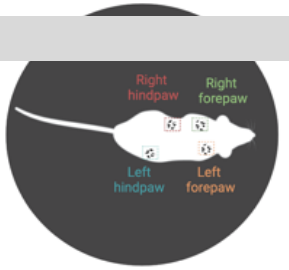

G

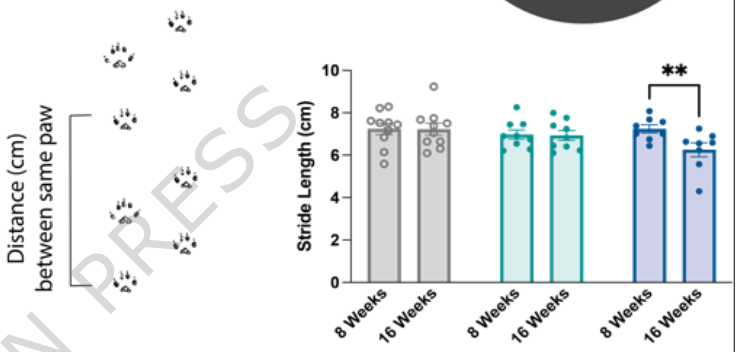

H

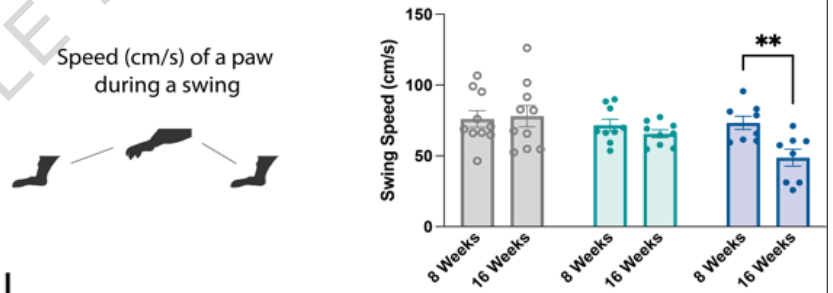

I